



Estimation of 3T MR Images from 1.5T Images Regularized with Physics Based Constraint

Prabhjot Kaur¹✉, Atul Singh Minhas², Chirag Kamal Ahuja³,
and Anil Kumar Sao⁴

¹ Indian Institute of Technology Mandi, Mandi, India
kaurprabhjotinresearch@gmail.com

² Magnetica, Northgate, Australia

³ Postgraduate Institute of Medical Education and Research, Chandigarh, India

⁴ Indian Institute of Technology Bhilai, Bhilai, India

Abstract. Limited accessibility to high field MRI scanners (such as 7T, 11T) has motivated the development of post-processing methods to improve low field images. Several existing post-processing methods have shown the feasibility to improve 3T images to produce 7T-like images [3, 18]. It has been observed that improving lower field (LF, ≤ 1.5 T) images comes with additional challenges due to poor image quality such as the function mapping 1.5T and higher field (HF, 3T) images is more complex than the function relating 3T and 7T images [10]. Except for [10], no method has been addressed to improve ≤ 1.5 T MRI images. Further, most of the existing methods [3, 18] including [10] require example images, and also often rely on pixel to pixel correspondences between LF and HF images which are usually inaccurate for ≤ 1.5 T images. The focus of this paper is to address the unsupervised framework for quality improvement of 1.5T images and avoid the expensive requirements of example images and associated image registration. The LF and HF images are assumed to be related by a linear transformation (LT). The unknown HF image and unknown LT are estimated in alternate minimization framework. Further, a physics based constraint is proposed that provides an additional non-linear function relating LF and HF images in order to achieve the desired high contrast in estimated HF image. This constraint exploits the fact that the T1 relaxation time of tissues increases with increase in field strength, and if it is incorporated in the LF acquisition the HF contrast can be simulated. The experimental results demonstrate that the proposed approach provides processed 1.5T images, i.e., estimated 3T-like images with improved image quality, and is comparably better than the existing methods addressing similar problems.

This work is financially supported by Ministry of Electronics and Information Technology, India.

Supplementary Information The online version contains supplementary material available at https://doi.org/10.1007/978-3-031-43999-5_13.

The improvement in image quality is also shown to provide better tissue segmentation and volume quantification as compared to scanner acquired 1.5T images. The same set of experiments have also been conducted for 0.25T images to estimate 1.5T images, and demonstrate the advantages of proposed work.

Keywords: Low field MRI · 0.25T · 1.5T · 3T · T1 relaxation times · Optimization

1 Introduction

Magnetic resonance imaging (MRI) has seen a tremendous growth over the past three decades as a preferred diagnostic imaging modality. Starting with the 0.25T MRI scanners in 1980s [11], clinical scanners have emerged from 1.5T and 3T to the recently approved 7T scanners [9]. Primary reason for the preference of higher magnetic field strength (FS) is the better image quality but it comes with high cost. Generally, the cost of clinical MRI scanners increases at USD 1million/Tesla [14]. Therefore, there is a clear divide in the distribution of MRI scanners across different countries in the world. With the FDA approval of clinical use of 7T MRI scanners- 3T and 7T MRI scanners have become preferred scanners in developed countries but inexpensive low field MRI scanners ($<1\text{T}$) and mid field MRI scanners (1.5T) are still a popular choice in developing countries [10, 11].

Since the past decade, there is a growing interest towards improving the quality of images acquired with low FS MRI scanners by learning the features responsible for image quality from high FS MRI scanners [8, 9, 19]. Earlier methods in such image translational problems synthesized target image contrast using paired example images [13]. The first work to address estimation of 7T-like images was reported in 2016 [1]. It exploits canonical correlation analysis (CCA) [5] to relate paired 3T-7T images in a more correlated space. With advent of deep learning, 3D convolutional neural network (CNN) was proposed to learn non-linear mapping between 3T and 7T images [3]. Different architectures of deep learning were addressed with better performances than previous methods [2, 7, 8, 18]. However, except Lin et al [10], none of the existing approaches address the problem of improving the image quality of $\leq 1.5\text{T}$ images to estimate high quality 3T-like MR images. Notably, to the best of our knowledge no approach is reported in literature to estimate the 3T (or 1.5T-like) images from 1.5T (or 0.25T) images. This problem is particularly challenging because of the severity of degradation present in $\leq 1\text{T}$ MR images [10]. In [10], the mapping between example 3T and simulated 0.36T images using CNNs to estimate 3T from scanner-acquired 0.36T images is learned, and it requires the a-priori knowledge of distribution of tissue-specific SNR for given FS. Since the databases for example images are scarce and SNR of tissues is not known a-priori [12], the unsupervised methods needs to be explored to improve $\leq 1.5\text{T}$ images.

In this work, we address the problem of estimating 3T-like images (\mathbf{x}) from 1.5T images (\mathbf{y}) in an unsupervised manner. To our best knowledge, this is the

first work to develop a method for improving $\leq 1.5\text{T}$ images to estimate HF images without requiring example images. The proposed method formulates the estimation of 3T HF images as an inverse problem: $\mathbf{y} = f(\mathbf{x})$, where $f(\cdot)$ is the unknown degradation model. The novel contributions of our work are as follows: (i) the alternate minimization (AM) framework is formulated to estimate \mathbf{x} as well as the mapping kernel $f(\cdot)$ relating \mathbf{x} and \mathbf{y} , (ii) Acquisition physics based signal scaling is proposed to synthesize the desired image contrast similar to HF image, (iii) the simulated contrast image is used as a regularizer while estimating \mathbf{x} from \mathbf{y} . The experimental results demonstrate that the proposed approach provides improved quality of MRI images in terms of image contrast and sharp tissue boundaries that is similar to HF images. The experiments further demonstrate the successful application of the improved quality images provided by proposed method in improved tissue segmentation and volume quantification.

2 Proposed Method

The proposed work formulates the estimation of HF image (\mathbf{x}) from LF image (\mathbf{y}) in an alternate minimization framework:

$$\min_{\mathbf{h}, \mathbf{x}} \underbrace{\|\mathbf{y} - \mathbf{h} * \mathbf{x}\|_F^2}_{\text{Data Fidelity}} + \lambda_1 \underbrace{\|\mathbf{c} \odot \mathbf{y} - \mathbf{x}\|_F^2}_{\text{Physics based Regularizer}} + \lambda_2 \underbrace{\|\mathbf{h}\|_2^2}_{\text{Regularizing } \mathbf{h}} \quad (1)$$

Here $\mathbf{x} \in \mathbb{R}^{m \times n}$ and $\mathbf{y} \in \mathbb{R}^{m \times n}$ represent the HF and LF MRI images, respectively. The matrix $\mathbf{h} \in \mathbb{R}^{p \times p}$ represents transformation kernel convolved using $*$ operator with each patch of \mathbf{y} of size $p \times p$ and p is empirically chosen as 5. The matrix $\mathbf{c} \in \mathbb{R}^{m \times n}$ represent the pixel wise scale when multiplied with \mathbf{y} generates the image with contrast similar to HF image. Here, $\mathbf{c} \odot \mathbf{y}$ represents the Hadamard product of pixel wise scale \mathbf{c} and \mathbf{y} the 1.5T (or 0.25T) image.

2.1 Physics Based Regularizer

The physics based regularizer exploits the fact that the T1 relaxation time increases with FS. The differences among T1 relaxation times of gray matter (GM), white matter (WM) and cerebrospinal fluid (CSF) also increase with FS, leading to increased contrast in the T1-weighted images in the order $3\text{T} \geq 1.5\text{T} \geq 0.25\text{T}$. This factor is used to simulate an image from \mathbf{y} which convey similar information as \mathbf{x} , and is obtained by scaling the signal intensities of \mathbf{y} based on changes in signal due to changes in T1 relaxation time with respect to FS- denoted by \mathbf{r} . The acquired signal for \mathbf{y} denoted by \mathbf{s}_l can be corrected with relaxation time to simulate the signal \mathbf{s}_h that would have been acquired for \mathbf{x} as:

$$\hat{\mathbf{s}}_h = \mathbf{r} \times \mathbf{s}_l. \quad (2)$$

For example, in the spin echo (SE) pulse sequence, acquired signal can be represented as, $\mathbf{s} = \mathbf{A}B_0^2 \frac{(1 - e^{(-TR/T_1)\sin\theta})}{(1 - e^{(-TR/T_1)\cos\theta})} e^{(-TE/T_2)}$ [6, 16]. Here, \mathbf{A} represents the

proportionality constant. The field strengths for 3T (or 1.5T) and 1.5T (or 0.25T) scanners are denoted by B_0 . The factor \mathbf{r} for the given voxel for SE sequence by assuming long TE, and T2 to be same across different FS (assumption derived from literature [12]) be computed as

$$\frac{(1 - e^{(-TR_h/T_{1,h}) \sin \theta_h})}{(1 - e^{(-TR_h/T_{1,h}) \cos \theta_h})} / \frac{(1 - e^{(-TR_l/T_{1,l}) \sin \theta_l})}{(1 - e^{(-TR_l/T_{1,l}) \cos \theta_l})}. \quad (3)$$

Here, T_1 and T_2 represent the T1/T2 relaxation times, TR -repetition time, TE -echo time and θ -flip angle (FA). The parameters with subscript h and l represent the parameters used for HF and LF MRI acquisitions, respectively. Similarly, respective mathematical formulations can be used for other pulse sequences such as fast SE (FSE) and gradient echo (GRE). After computing \mathbf{r} using Eq. (3), it can be used to simulate HF acquisition $\hat{\mathbf{s}}_h$ using Eq. (2)

The values of T_1/T_2 relaxation times differ with tissues, hence different values of \mathbf{r} should be computed for every voxel considering the tissues present in that voxel. However, if we assign single tissue per voxel using any tissue segmentation technique such as FAST [15], compute \mathbf{r} for each voxel to estimate $\hat{\mathbf{s}}_h$, this could lead to discontinuity among tissue boundaries in simulated HF image, and is shown in Fig. S1 in supplementary material (SM).

Compute Relaxation Times for Voxels with More Than One Tissue:

In real practice there exist many voxels with more than one tissue kind present in them, and is the reason for discontinuities present in Fig. S1. The challenge is that T1 relaxation time for such voxels is not known that is required to estimate \mathbf{r} . We address this issue by estimating the T1 relaxation time of such voxel as linear combination of T1 relaxation times of tissues present in the given voxel. The linear weights are directly proportional to the probability of tissues present in the voxel. Though this work performs well with probability maps but we use pixel intensity to denote the probability of tissue to avoid the additional and expensive tissue segmentation step as follows: The top 5 percentile of pixel intensities are assumed to belong to WM and bottom 20 percentile as GM. Consider w and q as T1 relaxation time and corresponding pixel intensity, respectively. We here approximate relation between w and q using linear equation as $\frac{w_{WM} - w_{GM}}{q_{WM} - q_{GM}} = \frac{w - w_{GM}}{q - q_{GM}}$. Here, subscript indicates the tissue type. Here, w_{WM} and w_{GM} are T1 relaxation times which are currently assumed to be constant, and taken from literature [12] whereas q_{WM} and q_{GM} are the pixel intensity values computed by averaging pixel intensities falling in mentioned percentiles for WM and GM, respectively. In a simplest case, say for an image q_{WM} and q_{GM} are 1 and 0, then the linear relationship is reduced to $w = (w_{WM} - w_{GM})q + w_{GM}$. Hence, for the given pixel intensity we can estimate the corresponding T1 relaxation time as a linear combination of T1 relaxation times of WM and GM. The range of pixel intensities in \mathbf{y} is partitioned into several bins. This is followed by approximation of T1 relaxation times ($T_{1,l}$) for different bins for \mathbf{y} by assuming w_{WM} and w_{GM} as T1 relaxation times at LF FS. In the similar way, $T_{1,h}$ can be approximated.

After approximating $T_{1,l}$ and $T_{1,h}$ for all voxels (and empirically choosing the TR_h and θ_h) the \mathbf{r} is computed using Eq. (3) and is used to estimate the HF acquisition using Eq. (2). The estimated $\hat{\mathbf{s}}_h$ is used to compute the pixel wise scale \mathbf{c} as $\mathbf{c} = \hat{\mathbf{s}}_h/\mathbf{y}$, i.e., an element wise division operator. The computed \mathbf{c} is used in Eq. (1) to constrain the solution space of estimated HF image \mathbf{x} .

3 Experimental Results

The proposed work has been demonstrated for (i) estimating 3T-*like* from 1.5T images, (ii) estimating 1.5T-*like* from 0.25T images, (iii) evaluating accuracy of tissue segmentation using improved images in (i) and (ii), and (iv) comparing (i), (ii) and (iii) with existing methods. The results related to (ii) are summarized in SM due to space constraints. The values for λ_1 and λ_2 are chosen as 1.2 and 0.4, respectively.

3.1 Data

The MRI images used to demonstrate the efficacy of proposed work were acquired from five healthy subjects of age 25 ± 10 years. Three different MRI scanners were used in this study: 0.25T (G-scan Brio, Esaote), 1.5T (Aera Siemens) and 3T (Verio, Siemens). The first three subjects were scanned using each of the three scanners while the other two subjects were scanned with only 1.5T and 3T scanners. The three scanners were located in Post Graduate Institute of Medical Education & Research (PGIMER) Chandigarh, India. Scanning was performed using the standard clinical protocols-optimized for both clinical requirement and work-load of clinical site. All the scans were performed according to the guidelines of the Declaration of Helsinki. The details of pulse sequence and scan parameters used to acquire data in each of the three scanners is mentioned in SM Table S1. The acquired T1 MR image volumes for each scanner and each human subject were pre-processed similar to the human connectome project (HCP) pre-processing pipelines for structural MR images [4]. Please note that proposed approach does not require the LF and HF images to be skull stripped or to have pixel to pixel correspondence. It is only done to provide reference based similarity scores of estimated image with respect to HF image.

3.2 Analysis/Ablation Study of Proposed Approach

The HF image is estimated at different stages of proposed approach to demonstrate the significance of each term in Eq. (1), and is shown in Fig. 1(a). In Fig. 1(b), the impact of proposed regularizer on estimation of HF image is demonstrated by changing the values of λ_1 . It can be observed that the image Fig. 1(a)-(ii) obtained just from the data fidelity term leads to sharp image details but without any contrast improvement. However, HF image simulated by the physics based regularizer from Eq. (2) improves the contrast but details remain blurred, as is evident from image Fig. 1(a)-(iii). Once the data fidelity and the physics

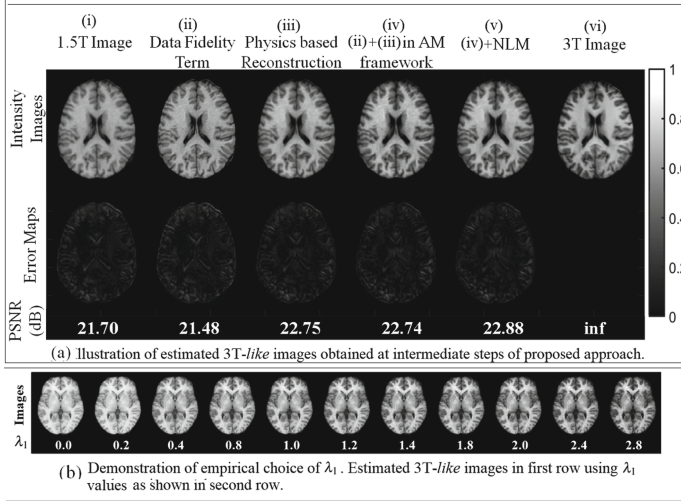


Fig. 1. (a) Ablation study of proposed approach. (b) Demonstration of significance of proposed physics based constraint and associated parameter λ_1 .

based regularizer is combined as in Eq. (1) in AM framework the corresponding image is shown in Fig. 1(a)-(iv) that is sharper as well as improved in contrast, and with image sharpness = 3.19, PIQE = 4.7, and SSIM = 0.0762. The image in Fig. 1(a)-(iv) is further smoothed in Fig. 1(a)-(v) using Non local means (NLM) approach to avoid any grainy effect if present due to division of pixel intensities into bins. The improvement in image quality is also evident from the PSNR values which increase from Fig. 1(a)-(ii) to (v).

3.3 Comparison with Existing Approaches

The performance of proposed approach is compared with existing methods that either address the contrast synthesis or estimation of HF images ScSR [17], CCA [5], MIMECS [13], ED [8]. The comparison is done in four ways: (i) *Objective analysis using reference based* metrics that requires the ground truth HF image, and pixel to pixel to correspondence between query image and ground truth image- Table 1, (ii) *Objective analysis using no-reference based* metrics which describe the quality of images solely based on edge sharpness and image contrast- Table 2, (i ii) *Subjective analysis* that includes rating of images by clinical experts in range 0 to 5, 5 and 0 being the highest and worst quality images, respectively - Table 3 and (iv) *Qualitative analysis* that includes the analysis of visual appearance of image details - Fig. 2. It can be observed that the existing methods provide better performance in terms of reference based metrics but perform inferior to proposed method in case of no-reference based metrics and subjective scores. This is due to the way the existing methods are designed, i.e., these methods are trained to minimize the mean square error

Table 1. OBJECTIVE ANALYSIS- NO-REFERENCE BASED METRICS

Metric		1.5T	HM	Supervised Approaches					Unsupervised Approaches		3T
				SCSR	CCA	MIMECS	EDp	ED	Proposed	Proposed (NLM)	
Signal Difference	WM-GM	0.1652	0.3414	0.1605	0.2079	0.2084	0.1291	0.1715	0.2166	0.2165	0.2449
	GM-CSF	0.3381	0.4536	0.3263	0.3154	0.3112	0.3345	0.3208	0.3207	0.3209	0.3144
Image Sharpness	Sharpness	55.62	95.16	58.09	54.81	54.25	60.39	52.06	63.01	64.13	64.6
	Edge width	0.1634	0.1559	0.1527	0.1837	0.1855	0.1545	0.1716	0.1812	0.1735	0.1776
	Edge height	9.08	14.81	8.87	10.07	10.06	9.32	8.93	11.42	11.12	11.46
PIQE	mean	67.57	60.63	51.52	74.32	75.86	58.76	82.81	57.78	72.53	70.25

Table 2. OBJECTIVE ANALYSIS- REFERENCE BASED METRICS

Metric		1.5T	HM	Supervised Approaches					Unsupervised Approaches		3T
				SCSR	CCA	MIMECS	EDp	ED	Proposed	Proposed (NLM)	
PSNR	mean	23.6	17.71	22.57	25.01	25.02	19.96	25.41	24.24	24.27	inf
	std.	0.1873	0.2244	0.1639	0.1441	0.1639	0.0426	0.1178	0.1849	0.1864	-
SSIM	mean	0.8314	0.8885	0.7639	0.8531	0.8465	0.6917	0.8511	0.8387	0.8465	1
	std.	0.0069	0.002	0.0047	0.0066	0.0072	0.0036	0.0058	0.0064	0.0064	-
UQI	mean	0.4854	0.8581	0.4300	0.6647	0.6607	0.4362	0.7053	0.5196	0.5263	1
	std.	0.101	0.0044	0.084	0.0275	0.0265	0.0065	0.0183	0.0755	0.095	-
VIF	mean	0.2697	0.5022	0.188	0.281	0.282	0.2784	0.3072	0.2451	0.251	1
	std.	0.0052	0.0074	0.002	0.0063	0.0063	0.0011	0.0067	0.0039	0.004	-

between estimated and HF images, thus they provide higher peak signal to noise ratio (PSNR) and structural similarity index metric (SSIM) but the image details are still blurred which lead to drop in edge sharpness. The validation of argument can also be derived by visually inspecting the images in Fig. 2. It has been observed that encoder-decoder based approach (ED [8]), MIMECS [13], CCA [5] and ScSR [17] provides blurred image details. The possible reasons are (i) minimizing MSE can provide perceptually blurred results, (ii) the weighted averaging involved in [5, 13, 17] induces blur, (iii) inaccurate pixel to pixel correspondences makes it difficult for supervised methods to learn the actual mapping relating input and target images. The drop in performances of existing approaches due to inaccuracies in image registration is more prominently observed when improving 0.25T images in Fig. S3. The robustness to such inaccuracies by proposed approach due to its unsupervised nature shows its clear advantages over existing methods.

Table 3. SUBJECTIVE ANALYSIS

Expert	1.5T	HM	Supervised Approaches					Unsupervised Approaches		3T
			SCSR	CCA	MIMECS	EDp	ED	Proposed	Proposed (NLM)	
(i)	3.25	4	2.5	4	4	2.25	3	4	4.25	5
(ii)	1	3	3	4	3	3	2	4	4	5
(iii)	1.75	3.75	1.5	0.75	1.5	0	2.25	5	4	4
(iv)	3.5	2.75	2.5	1.5	2	0	2.25	4.25	3	4.25
(v)	0.25	5	0.25	2	2.25	3	1.25	5	4.25	4.25

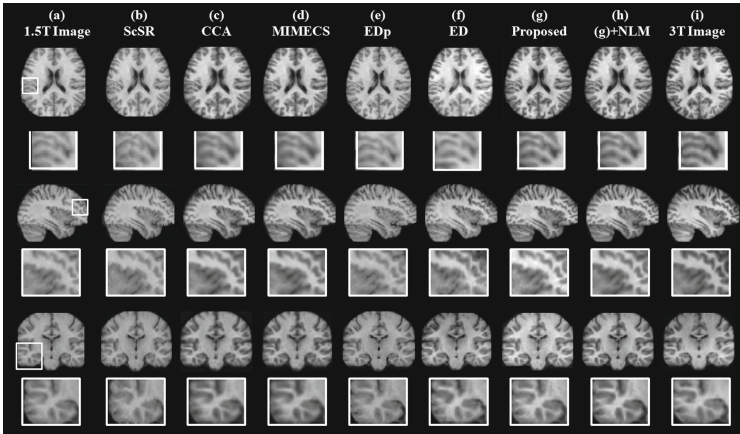


Fig. 2. Comparison of quality of HF images estimated by various methods.

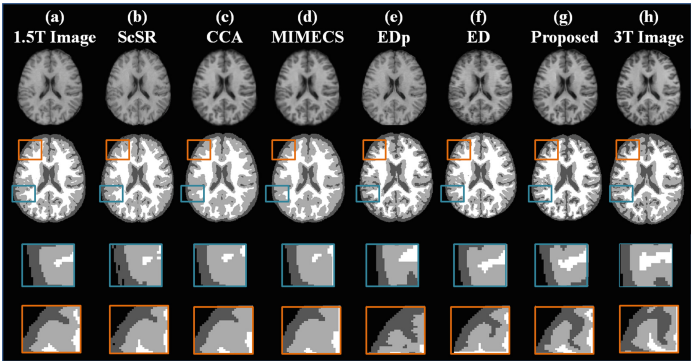


Fig. 3. Demonstration of improved segmentation from images estimated by proposed approach and its comparison with existing approaches

3.4 Application to Tissue Segmentation and Volume Quantification

The segmentation labels for WM, GM and CSF were computed using FAST toolbox in FSL software [15] for 3T-like images estimated by different approaches, and shown in Fig. 3. The improved tissue segmentation for 0.25T images is shown in Fig. S5 in SM. The zoomed windows in both figures indicate that the segmentation label of WM is improved for the estimated 3T reconstructed image by the proposed approach for estimated 3T image from 1.5T image. The quantitative measure used to evaluate performance of different methods is dice ratio, and is reported in Table S2, and its comparison is mentioned in Table S3. The ability to accurately segment tissues from image estimated by proposed approach is shown to be comparable both qualitatively and quantitatively to existing methods. Further, proposed method is shown to provide statistically significant with $p < 0.01$ improvement in accuracy of WM and GM tissue volume quantification for estimated 3T (and 1.5T images), and is shown in Fig. S6.

4 Summary

We propose a method to estimate HF images from ≤ 1.5 T images in an unsupervised manner. Here, the knowledge of acquisition physics to simulate HF image is exploited, and used it in a novel way to regularize the estimation of HF image. The proposed method demonstrates the benefits over state of the art supervised methods that are severely effected by the inaccuracies if present in image registration process. Lower the FS image is, harder is to get accurate image registration, and thus proposed method proves to be a better choice. Further, it is also demonstrated that the proposed approach provides statistically significant accurate tissue segmentation. The code for this work is publicly shared on <https://drive.google.com/drive/folders/1WbzkBJS1BWAje8aF0ty2SWYTQ9i0B7Yr?usp=sharing>.

References

1. Bahrami, K., Rekik, I., Shi, F., Gao, Y., Shen, D.: 7T-guided learning framework for improving the segmentation of 3T MR images. In: Ourselin, S., Joskowicz, L., Sabuncu, M.R., Unal, G., Wells, W. (eds.) MICCAI 2016. LNCS, vol. 9901, pp. 572–580. Springer, Cham (2016). https://doi.org/10.1007/978-3-319-46723-8_66
2. Bahrami, K., Rekik, I., Shi, F., Shen, D.: Joint reconstruction and segmentation of 7T-like MR images from 3T MRI based on cascaded convolutional neural networks. In: Descoteaux, M., Maier-Hein, L., Franz, A., Jannin, P., Collins, D.L., Duchesne, S. (eds.) MICCAI 2017. LNCS, vol. 10433, pp. 764–772. Springer, Cham (2017). https://doi.org/10.1007/978-3-319-66182-7_87
3. Bahrami, K., Shi, F., Rekik, I., Shen, D.: Convolutional neural network for reconstruction of 7T-like images from 3T MRI using appearance and anatomical features. In: Carneiro, G., et al. (eds.) LABELS/DLMIA-2016. LNCS, vol. 10008, pp. 39–47. Springer, Cham (2016). https://doi.org/10.1007/978-3-319-46976-8_5
4. Glasser, M.F., et al.: The minimal preprocessing pipelines for the human connectome project. *Neuroimage* **80**, 105–124 (2013). Mapping the Connectome

5. Huang, H., He, H., Fan, X., Zhang, J.: Super-resolution of human face image using canonical correlation analysis. *Pattern Recogn.* **43**(7), 2532–2543 (2010)
6. Jung, B.A., Weigel, M.: Spin echo magnetic resonance imaging. *J. Magn. Reson. Imaging* **37**(4), 805–817 (2013)
7. Kaur, P., Sao, A.K.: Single Image based reconstruction of high field-like MR images. In: Shen, D., et al. (eds.) *MICCAI 2019*. LNCS, vol. 11766, pp. 74–82. Springer, Cham (2019). https://doi.org/10.1007/978-3-030-32248-9_9
8. Kaur, P., Sharma, A., Nigam, A., Bhavsar, A.: MR-SRNET: transformation of low field MR images to high field MR images. In: *25th IEEE International Conference on Image Processing (ICIP)*, pp. 2057–2061, October 2018
9. der Kolk, A.G.V., Hendrikse, J., Zwanenburg, J.J., Visser, F., Luijten, P.R.: Clinical applications of 7T MRI in the brain. *Eur. J. Radiol.* **82**(5), 708–718 (2013)
10. Lin, H., et al.: Deep learning for low-field to high-field MR: image quality transfer with probabilistic decimation simulator. In: Knoll, F., Maier, A., Rueckert, D., Ye, J.C. (eds.) *MLMIR 2019*. LNCS, vol. 11905, pp. 58–70. Springer, Cham (2019). https://doi.org/10.1007/978-3-030-33843-5_6
11. Marques, J.P., Simonis, F.F., Webb, A.G.: Low-field MRI: an MR physics perspective. *J. Magn. Reson. Imaging* **49**(6), 1528–1542 (2019)
12. Nishimura, D.: *Principles of Magnetic Resonance Imaging*. Stanford (2010)
13. Roy, S., Carass, A., Prince, J.L.: Magnetic resonance image example-based contrast synthesis. *IEEE Trans. Med. Imaging* **32**(12), 2348–2363 (2013)
14. Sarraçanie, M., Salameh, N.: Low-field MRI: how low can we go? A fresh view on an old debate. *Front. Phys.* **8**, 1–14 (2020)
15. Shi, F., Wang, L., Dai, Y., Gilmore, J.H., Lin, W., Shen, D.: Label: Pediatric brain extraction using learning-based meta-algorithm. *Neuroimage* **62**(3), 1975–1986 (2012)
16. Wu, Z., Chen, W., Nayak, K.S.: Minimum field strength simulator for proton density weighted MRI. *PLoS ONE* **11**(5), 1–15 (2016)
17. Yang, J., Wright, J., Huang, T.S., Ma, Y.: Image super-resolution via sparse representation. *IEEE Trans. Image Process.* **19**(11), 2861–2873 (2010)
18. Zhang, Y., Cheng, J.-Z., Xiang, L., Yap, P.-T., Shen, D.: Dual-domain cascaded regression for synthesizing 7T from 3T MRI. In: Frangi, A.F., Schnabel, J.A., Davatzikos, C., Alberola-López, C., Fichtinger, G. (eds.) *MICCAI 2018*. LNCS, vol. 11070, pp. 410–417. Springer, Cham (2018). https://doi.org/10.1007/978-3-030-00928-1_47
19. van der Zwaag, W., Schäfer, A., Marques, J.P., Turner, R., Trampel, R.: Recent applications of UHF-MRI in the study of human brain function and structure: a review. *NMR Biomed.* **29**(9), 1274–1288 (2016)